ISSN 1674-1056
http://cpb.iphy.ac.cn
http://iopscience.iop.org/cpb
中国物理 B
Chinese Physics
中国物理
Chinese Physics B

Treatable focal region modulated by double excitation signal superimposition to realize platform temperature distribution during transcranial brain tumor therapy with high-intensity focused ultrasound

Shi-Hui Chang(常诗卉), Rui Cao(曹睿), Ya-Bin Zhang(张亚斌), Pei-Guo Wang(王佩国), Shi-Jing Wu(吴世敬), Yu-Han Qian(钱宇晗), Xi-Qi Jian(菅喜岐)

Citation: Chin. Phys. B . 2018, 27(7): 078701. **doi:** 10.1088/1674-1056/27/7/078701

Journal homepage: http://cpb.iphy.ac.cn; http://iopscience.iop.org/cpb

What follows is a list of articles you may be interested in

Effect of focused ultrasound stimulation at different ultrasonic power levels on the local field potential power spectrum

Yuan Yi, Lu Cheng-Biao, Li Xiao-Li

Chin. Phys. B . 2015, 24(8): 088704. **doi:** 10.1088/1674-1056/24/8/088704

Treatable focal region modulated by double excitation signal superimposition to realize platform temperature distribution during transcranial brain tumor therapy with high-intensity focused ultrasound*

Shi-Hui Chang(常诗卉)[1], Rui Cao(曹睿)[2], Ya-Bin Zhang(张亚斌)[1,3], Pei-Guo Wang(王佩国)[4], Shi-Jing Wu(吴世敬)[1], Yu-Han Qian(钱宇晗)[1], and Xi-Qi Jian(菅喜岐)[1,†]

[1] *School of Biomedical Engineering and Technology, Tianjin Medical University, Tianjin* 300070, *China*
[2] *College of Mechanical Engineering, Tianjin University of Science & Technology, Tianjin* 300222, *China*
[3] *Union Stem Cell & Gene Engineering Co., Ltd., Tianjin* 300384, *China*
[4] *Tianjin Medical University Cancer Institute and Hospital, Tianjin* 300060, *China*

(Received 2 February 2018; revised manuscript received 1 May 2018; published online 25 June 2018)

Recently, the phase compensation technique has allowed the ultrasound to propagate through the skull and focus into the brain. However, the temperature evolution during treatment is hard to control to achieve effective treatment and avoid over-high temperature. Proposed in this paper is a method to modulate the temperature distribution in the focal region. It superimposes two signals which focus on two preset different targets with a certain distance. Then the temperature distribution is modulated by changing triggering time delay and amplitudes of the two signals. The simulation model is established based on an 82-element transducer and computed tomography (CT) data of a volunteer's head. A finite-difference time-domain (FDTD) method is used to calculate the temperature distributions. The results show that when the distances between the two targets respectively are 7.5–12.5 mm on the acoustic axis and 2.0–3.0 mm in the direction perpendicular to the acoustic axis, a focal region with a uniform temperature distribution (64–65 °C) can be created. Moreover, the volume of the focal region formed by one irradiation can be adjusted (26.8–266.7 mm^3) along with the uniform temperature distribution. This method may ensure the safety and efficacy of HIFU brain tumor therapy.

Keywords: high-intensity focused ultrasound (HIFU), transcranial therapy, double excitation signal superimposition, temperature modulation of focal region

PACS: 87.50.Y–, 87.55.Gh, 87.55.dh, 87.55.de **DOI:** 10.1088/1674-1056/27/7/078701

1. Introduction

In recent years, using ultrasound as a treatment modality has been increasingly widespread.[1–4] High-intensity focused ultrasound (HIFU) as a new technique to treat tumors has received a great deal of attention because it is noninvasive or minimally invasive. Also it can concentrate the ultrasound energy in a target area deeply seated in the human body and achieve the treatment purpose repeatedly. The HIFU has been used clinically to treat some solid tumors[5–7] such as uterine fibroid, breast carcinoma, prostatic cancer, etc. However, acoustic energy is difficult to deposit in the deeply seated brain tissue. The reason is attributed to the acoustic impendence of the skull. The absorption and attenuation of the skull are both strong. In early studies,[8,9] the researchers even removed part of the skull to enhance the ultrasound deposition on the target in the brain. With the development of the phased array transducer, ultrasound can propagate through the skull and focus into deep brain tissue using the adaptive focusing techniques.[10–14] However, its feasibility and safety are not ideal since temperature rise in the target area is difficult to control.

With the development of the phase compensation technique of sound wave and medical imaging technology, the HIFU is improved to penetrate the skull by researchers. In the 1990s, the research about the phase correcting technique showed that transcranial brain tumor treatment using HIFU was feasible.[11,14,15] From the end of the last century to recent years, the structure and parameter information of skull captured from medical imaging provided help for the simulation of transcranial HIFU.[12,16–18] The simulations and *ex vivo* verification experiments further demonstrated the feasibility of HIFU in transcranial brain tumor treatment. At the same time, studies showed that the hemispheric phased array transducer could maximize the penetration area of ultrasound on the skull surface and reduce the thermal deposition in the skull.[19] The proposition of hot spot eliminating algorithm and amplitude compensation helped to lower the temperature in the skull and raise the temperature at the target location.[10,13,20] The HIFU was implemented in some clinical trials to treat patients suffering from glioma, tremor, chronic neuralgia, etc. Some treatments were successful in partial tumor ablation,[21] reduced neuropathic pain,[22] and diminished tremor.[23,24] However,

*Project supported by the National Natural Science Foundation of China (Grant No. 81272495) and the Natural Science Foundation of Tianjin, China (Grant No. 16JC2DJC32200).

†Corresponding author. E-mail: jianxiqi@tmu.edu.cn

© 2018 Chinese Physical Society and IOP Publishing Ltd

some treatments did not achieve the desired results.[22,24,25]

The focal temperature control in HIFU brain tumor treatment is critical. It affects the therapeutic efficacy directly. If the target area in the brain is overheated, it will be dangerous to the patient.[22,26] On the other hand, the treatment may be in vain if the focal temperature is insufficient.[23,27] In order to control the thermal deposition in the treatment volume, Ebbini and Cain used the pseudoinverse method to compute the array element amplitude and phase distributions to form multiple foci with desired levels at a set of control points in 1989.[28] Salomir *et al.* obtained a uniform temperature distribution within a large target volume using a double spiral trajectory of the transducer focal point in 2000.[29] Lu *et al.* proposed a multi-objective control method to generate an ideal spatial energy distribution for HIFU surgery.[30,31] Partanen *et al.* combined a multi foci sonication approach with a mild hyperthermia heating algorithm and achieved precise heating within the targeted region in 2013.[32] Zhou attempted to obtain uniformly distributed ultrasound energy in the target area by optimizing the irradiation path and time interval between irradiations in 2013.[33] The temperature distribution and volume of the focal region could be changed by electronic beam steering using a phased array transducer.[34,35] However, it is restricted more or less by the skull when HIFU is used to treat brain tumors.

In the present study, a new technique for modulating the transcranial temperature distribution of the focal region is proposed. In this technique, two targets are set to be either on the acoustic axis or perpendicular to the acoustic axis with a certain distance. As a result, two sets of excitation signals which focus on the two preset targets can be obtained using the time reversal method. The double signals are superimposed to stimulate each of the 82 elements of the transducer. The temperature distribution in the focal region is modulated by changing the triggering time delay and amplitudes of the two signals. Thus, a uniform thermal field is generated in the focal zone. The three-dimensional(3D) numerical simulation model is established based on an 82-element transducer and CT data of a 46 year-old male volunteer's head. The simulations based on the FDTD method are implemented to calculate the thermal field formed by dual-signal superimposed triggering HIFU, also to test if the new method is able to build an ideal focal region with effective uniform temperature distribution.

2. Methods

2.1. Simulation model

Figure 1 shows the transcranial HIFU brain tumor treatment simulation model and the ultrasound wave propagated into the brain from the top of head. The model is comprised of a transducer, water, skull and brain tissue. The phased array transducer consisted of 82 elements randomly lying on the spherical surface with 80 mm curvature radius and 100 mm diameter. The diameter of each element was 8 mm. The operating frequency of the transducer was 0.7 MHz. In the simulation, the calculation volume was a cube with $100 \times 100 \times 100$ mm. The origin of coordinates is shown in Fig. 1 and meanwhile the z-axis is the acoustic axis. The inner surface of the skull that was closest to the origin and at $z = 55$ mm. Simulations were performed with the 3D FDTD method, in which the spatial step was set to be 0.25 mm and the temporal step was 10 ns.

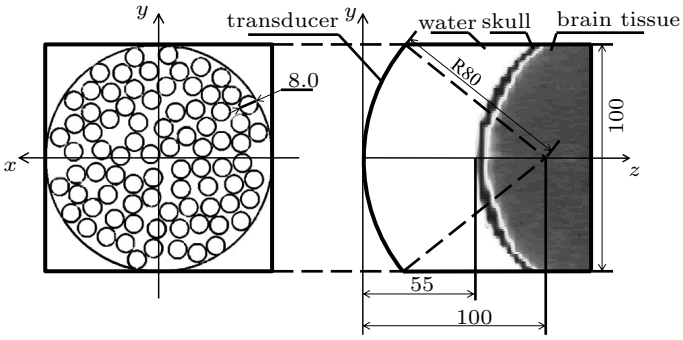


Fig. 1. 3D simulation model (unit: mm).

2.2. Basic equations used for calculating acoustic and thermal fields

In the simulations, the acoustic nonlinear propagation was described by the Westervelt equation written as[36,37]

$$\nabla^2 p - \frac{1}{c^2}\frac{\partial^2 p}{\partial t^2} + \frac{\delta}{c^4}\frac{\partial^3 p}{\partial t^3} + \frac{\beta}{\rho c^4}\frac{\partial^2 p^2}{\partial t^2} = 0. \tag{1}$$

In this equation, ∇ is the Laplace operator, p (Pa) is the acoustic pressure, t (s) is the time, ρ (kg/m^3) and c (m/s) are the density and sound velocity of the acoustic medium respectively, β is the nonlinear coefficient, δ is the acoustic diffusion coefficient and $\delta = 2c^3\alpha/\omega^2$ where α (dB/mm) is the acoustic attenuation coefficient, $\omega = 2\pi f$ (rad/s) is angular frequency and f is the drive frequency of the transducer.

The temperature distribution was calculated through the Pennes' bio-heat conduction equation written as[38,39]

$$\rho C_r \frac{\partial T}{\partial t} = r\nabla^2 T + Q - W_{\mathrm{B}} C_{\mathrm{B}} T, \tag{2}$$

where T is the temperature elevated from 37 °C, C_r (J/(kg·°C)) and r (W/(m·°C)) are the specific heat and the thermal conductivity of the medium respectively, W_{B} and C_{B} are the perfusion rate and heat capacity of blood, respectively. In the absence of blood perfusion, Pennes' bio-heat conduction equation can be reduced to

$$\frac{\partial T}{\partial t} = \frac{r}{\rho C_r}\nabla^2 T + \frac{1}{\rho C_r} Q. \tag{3}$$

Here, Q is the volumetric energy loss which is equal to $2\alpha I$, where $I = \frac{1}{t_{\mathrm{p}}}\int_0^{t_{\mathrm{p}}} \frac{p^2}{\rho c}\mathrm{d}t$ and t_{p} is the acoustic wave period.

The equivalent thermal dose t_{43}[40] was calculated from the following equation:

$$t_{43} = \int_{t_0}^{t_{\mathrm{final}}} \mathrm{R}^{43-T_i}\mathrm{d}t, \tag{4}$$

where T_t is the temperature after t-second irradiation, t_0 and t_{final} are the start time and finish time of the irradiation respectively, R is a constant, if $T_t >= 43$ °C, $R = 0.5$ and if $T_t < 43$ °C, $R = 0.25$.

2.3. Simulation parameters

In this study, the parameters of skull and brain tissue such as ρ, c, α were obtained based on the high resolution CT of a 46 year-old male volunteer's head provided by Tianjin Medical University Cancer Institute and Hospital. This study was approved by the ethics committee of Tianjin Medical University, Tianjin, China, and written informed consent was obtained from the volunteer. The CT scan parameters were 120 kV and 135 mA. The slice thickness and spacing were both 3 mm. To satisfy the spatial step of the simulation, a linear interpolation was performed between each slice of CT images.

The parameters were obtained from bone porosity (ϕ) converted from the Hounsfield unit (H) of the CT images and the calculation method was as follows:[16]

$$\phi = 1 - \frac{H}{1000}, \tag{5}$$

$$\rho = \phi \times \rho_{\text{water}} + (1-\phi) \times \rho_{\text{bone}}, \tag{6}$$

$$c = c_{\text{water}} + (1-\phi) \times (c_{\text{bone}} - c_{\text{water}}), \tag{7}$$

$$\alpha = \alpha_{\text{water}} + \phi^{0.5} \times (\alpha_{\text{bone}} - \alpha_{\text{water}}). \tag{8}$$

Here, ρ_{bone}, c_{bone}, and α_{bone} are density, speed of sound, and attenuation of cortical bone respectively; ρ_{water}, c_{water}, and α_{water} are density, speed of sound, and attenuation of water, respectively. The constant parameters used in the simulation[10,16,17] are shown in Table 1.

Table 1. Constant parameters used in simulation.

	ρ/kg·m^{-3}	c/m·s^{-1}	α/dB·mm^{-1}	β	r/W·m^{-1}·°C^{-1}	C_r/J·kg^{-1}·°C^{-1}
Water	998	1500	0.2	3.50	0.54	4180
Cortical skull	1600	3200	8.0	4.40	1.30	1840
Brain	–	–	–	4.60	0.52	3700

2.4. Phase and amplitude modulation of element driving signal

Here, F_1 and F_2 were set to be two different focal targets. The spacing between F_1 and F_2 was L as shown in Figs. 2(a) or 2(b). A point acoustic source $S_0(t) = I_0 \sin(\omega t)$ was set to be at F_1. Then a series of time-reversal signals could be recorded on the elements of the transducer based on the time reversal method. After that an arbitrary element was chosen as a reference and its time-reversal signal underwent self-correlation and cross-correlations with the time-reversal signals recorded on other elements to correct the phase and compensate for the amplitude of the excitation signals[10] that they could focus at F_1. The signal focusing at F_1 was

$$S_{1i}(t) = I_{1i} \sin(\omega t + \varphi_{1i}), \tag{9}$$

where φ_{1i} is the initial phase of the excitation signal on each transducer element and the subscript i refers to the element number, and I_{1i} is the acoustic intensity on each element. Similarly, an excitation signal that can focus at F_2 could be obtained to be

$$S_{2i}(t) = I_{2i} \sin(\omega t + \varphi_{2i}). \tag{10}$$

The two signals were superimposed to realize their focusing at F_1 and F_2 at the same time:

$$S_i(t) = M S_{1i}(t - \Delta t) + (1 - M) S_{2i}(t), \quad 0 \leqslant \Delta t \leqslant \frac{2\pi}{\omega}, \tag{11}$$

where Δt is the delay between the trigger times of $S_{1i}(t)$ and $S_{2i}(t)$, M is the modulation coefficient of the amplitude. M was equal to 0.50 when the total acoustic power on the 82 elements for S_{1i} and S_{2i} were the same.

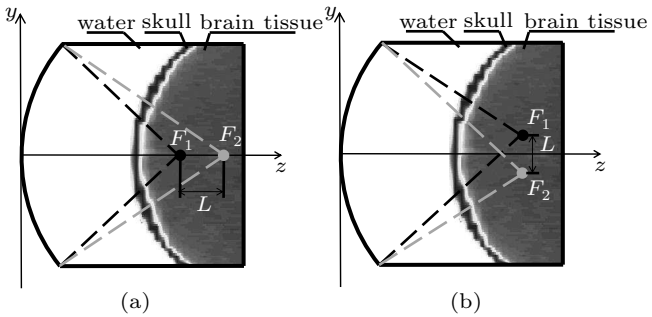


Fig. 2. Schematic of preset targets (a) both on the acoustic axis, and (b) on each side of the acoustic axis.

3. Results

3.1. Modulation with targets on acoustic axis

3.1.1. Modulation of Δt for controlling thermal field

In this study, 55 °C is selected as the threshold of protein denaturation.[21,25] Unless otherwise indicated, the maximum temperature is no more than 65 °C since some side effects can be induced at over high temperature.[41] First of all, the simulations with the targets set to be on the acoustic axis (as Fig. 2(a) shows) and F_1 located at (0, 0, 75), F_2 located at (0, 0, 85) ($L = 10$ mm) are implemented. The temperature distributions with different values of Δt (the acoustic power on the transducer $P_w = 103.05$ W and the amplitude modulation coefficient $M = 0.50$), when the maximum focal temperature reaches 65 °C, are shown in Fig. 3. One continuous focal region where the temperature is over 55 °C is formed when Δt = 0–400 ns. Two elliptic focal zones are formed when Δt = 600–800 ns. As the focal region is separated into two parts, the irradiation time for reaching 65 °C turns longer and the temperature at the skull correspondingly becomes higher. A continuous focal region appears again when $\Delta t > 1000$ ns.

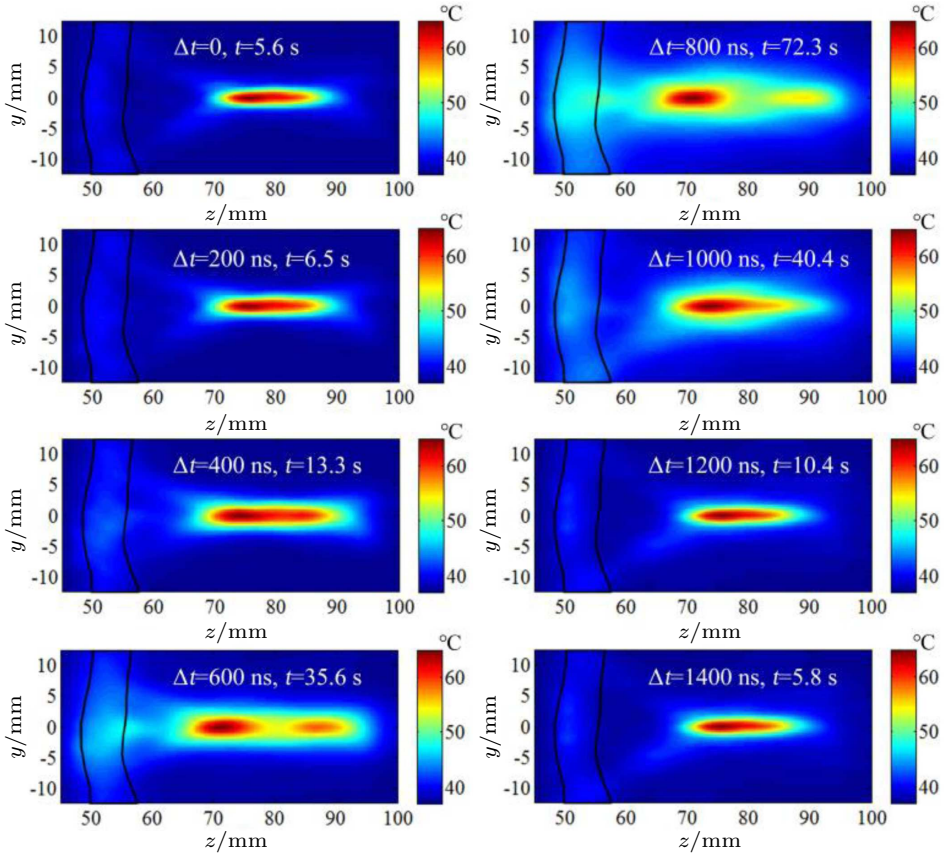


Fig. 3. (color online) Temperature distributions with different values of Δt in an acoustic wave period with targets both set on acoustic axis and maximum focal temperature of 65 °C ($L = 10.0$ mm, $M = 0.50$, and $P_w = 103.05$ W).

3.1.2. Amplitude modulation for generating uniform thermal field along acoustic axis

Taking the situation of $L = 10.0$ mm, $\Delta t = 400$ ns and $M = 0.50$ for example, the temperature distribution along the acoustic axis is marked as the blue curve shown in Fig. 4(a). Two peak temperatures T_1 and T_2 appear on the acoustic axis, and the distance between their locations is Δz_T. The difference between the valley temperature and maximum temperature is ΔT_m. In order to reduce ΔT_m, the value of M changes gradually. The temperature field when $M = 0.46$ is shown in Fig. 4(b) and the corresponding temperature curve along the acoustic axis is marked as the pink curve shown in Fig. 4(a). The value of ΔT_m decreases to 2.1 °C when the two peak temperatures are equal ($T_1 = T_2$) and it is 4.5 °C before M is modulated.

The values of M for $T_1 = T_2$ with different values of Δt when the temperature reaches 65 °C are shown in Fig. 5. The black curve represents the simulated values of M for $|T_1 - T_2| \leqslant 0.05$ °C. The values marked as the gray curve are computed from the following equation considering the effect of skull:

$$M = \frac{\sqrt{(T_2 - T_0)}}{\sqrt{(T_1 - T_0)} + \sqrt{(T_2 - T_0)}} - 10^{-0.1\Delta z_T} \int_0^{\overline{D}} 10^{-2\overline{\alpha}z} \mathrm{d}z. \tag{12}$$

The first item in the above equation is derived from Pennes' bio-heat conduction equation considering neither the influence of skull nor the thermal conduction between the adjacent tissues. When the effect of skull is considered, a process of gradually approximating the simulation results is implemented by adding the skull parameters into the equation. When the mean

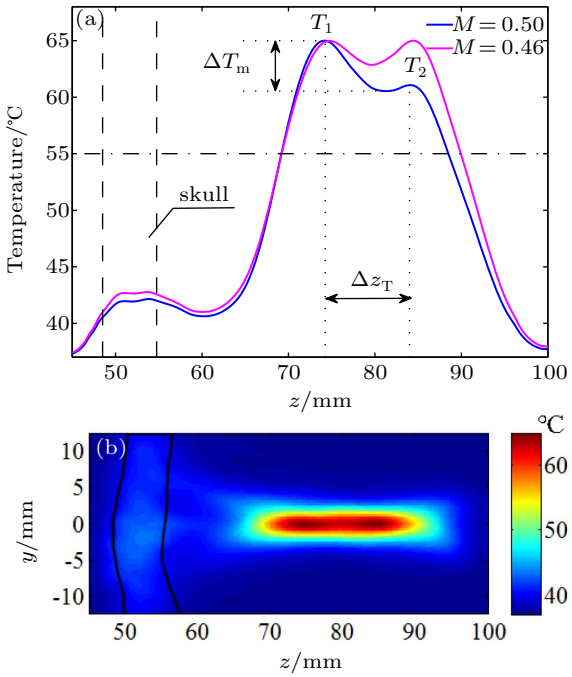


Fig. 4. (color online) Temperature distributions with $L = 10.0$ mm, $\Delta t = 400$ ns and $P_w = 103.05$ W when the maximum temperature reached 65 °C. (a) Temperature along the acoustic axis with $M = 0.50$ and $M = 0.46$. (b) Temperature distribution of the y–z plane of $x = 0$ with $M = 0.46$.

thickness $\overline{D}$ and the mean acoustic attenuation coefficient $\overline{\alpha}$ of the skull in the acoustic window are added as shown in Eq. (12), the simulated values of M match well with the computed ones.

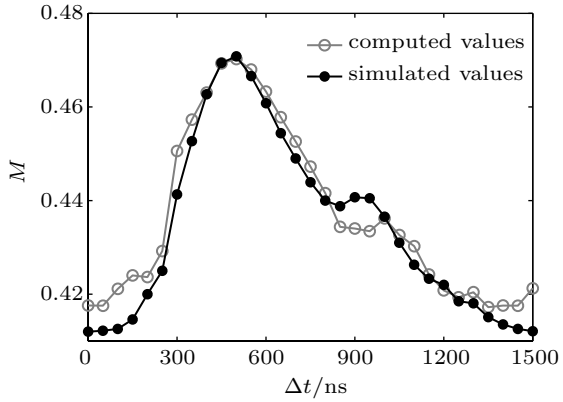


Fig. 5. Values of M for $T_1 = T_2$ varying with Δt in an acoustic wave period when the maximum temperature reaches 65 °C ($L = 10.0$ mm, $P_w = 103.05$ W).

Figure 6(a) shows the variation of Δz_T with Δt when $M = 0.50$. The values of ΔT_m after M has been modulated for $|T_1 - T_2| \leqslant 0.05$ °C, versus Δz_T are displayed in Fig. 6(b) (see gray circles). The relationship between ΔT_m and Δz_T can be fitted as (the goodness of fit $R_n^2 = 0.98$)

$$\Delta T_m = 0.233\, e^{0.225 \Delta z_T}. \tag{13}$$

If $\Delta T_m \leqslant 1$ °C is selected as a necessity for the uniform temperature distribution, $0 < \Delta z_T \leqslant 6.5$ mm can be obtained based on Eq. (13). The range of Δt that makes $0 < \Delta z_T \leqslant 6.5$ mm hold can be selected from Fig. 6(a) and the ranges of Δt are $0 \leqslant \Delta t \leqslant 200$ ns and 1150 ns $\leqslant \Delta t \leqslant 1400$ ns. The uniform temperature fields formed under that condition are shown in Fig. 7 and the volume of treatable focal region (TFR) where the thermal dose is more than 90 equivalent minutes at 43 °C[10,42] is 38.1–53.3 mm^3.

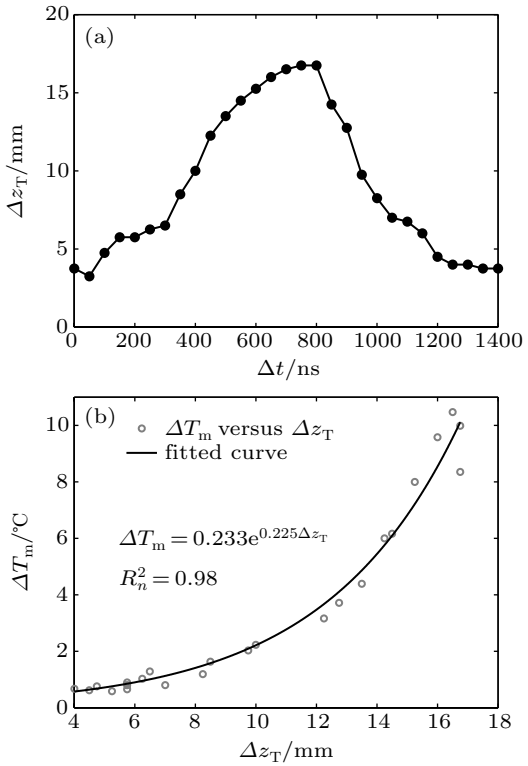


Fig. 6. (a) Variation of Δz_T with Δt when $M = 0.5$ and (b) variation of ΔT_m with Δz_T after M has been modulated ($L = 10.0$ mm, $P_w = 103.05$ W).

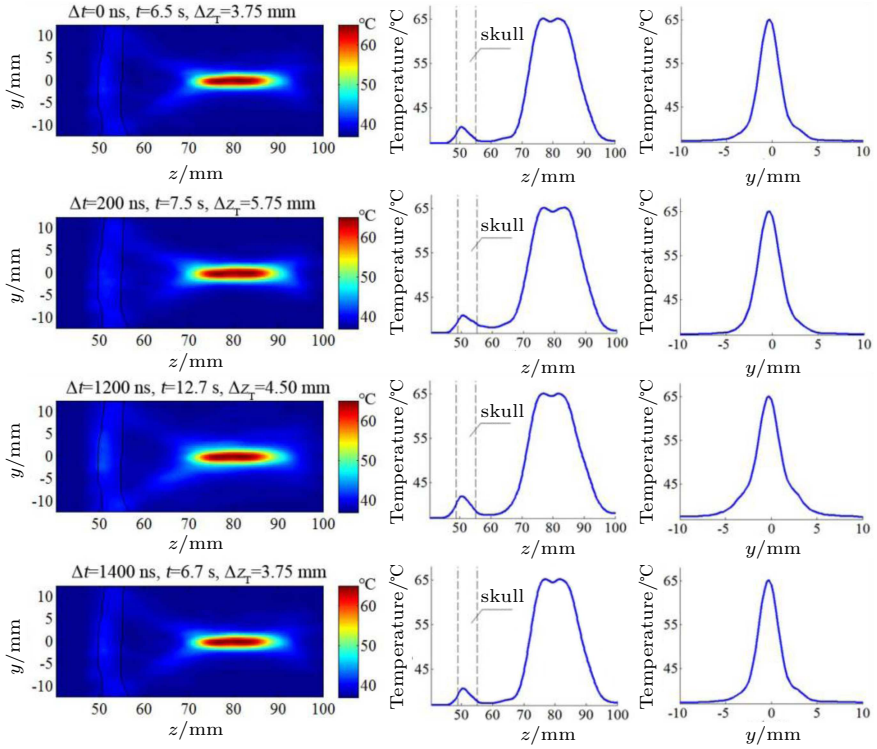


Fig. 7. (color online) Temperature distribution on the y–z plane of $x = 0$, along the acoustic axis and along the y direction across the position of the maximum temperature when the temperature field is uniform on the acoustic axis and the maximum focal temperature reaches 65 °C ($L = 10.0$ mm, $P_w = 103.05$ W).

3.1.3. Modulation for generating uniform temperature distribution along acoustic axis with different L values

The modulations for generating a uniform temperature distribution are implemented for different L values, with the location of F_1 fixed and the location of F_2 varied. Figure 8(a) shows the distance between the locations of the two peak temperatures in the thermal field of $P_w = 103.05$ W, $M = 0.50$ with different L values when the maximum focal temperature reaches 65 °C. The condition of $0 < \Delta z_T \leqslant 6.5$ mm can be satisfied when 7.5 mm $\leqslant L \leqslant$ 12.5 mm for generating a uniform temperature distribution with $\Delta T_m \leqslant 1$ °C. Figure 8(b) shows the variation of ΔT_m with L when M is modulated and the maximum focal temperature reaches 65 °C, where the curve represents the average ΔT_m obtained under certain L and corresponding value of Δt, and meanwhile the error bar displays the standard deviation. The blue curve displays the results modulated by the computed M from Eq. (12) and the pink curve shows the results modulated by the simulated M for $|T_1 - T_2| \leqslant 0.05$ °C. The largest difference between ΔT_m values obtained by the computed M and simulated M is 1.3 °C. After that the volume of TFR is computed with modulation that is done by the simulated M. The computed results are shown in Fig. 8(c). The range of Δt for generating a uniform temperature distribution turns narrow with L increasing. The volume of TFR is affected by Δt under the same L value. When Δt was the same, the volume of TFR becomes larger if L increases. Using the modulated focusing, the volume of focal region formed by one irradiation can be changed between 26.8 and 95.3 mm^3 when the temperature field is uniformly distributed.

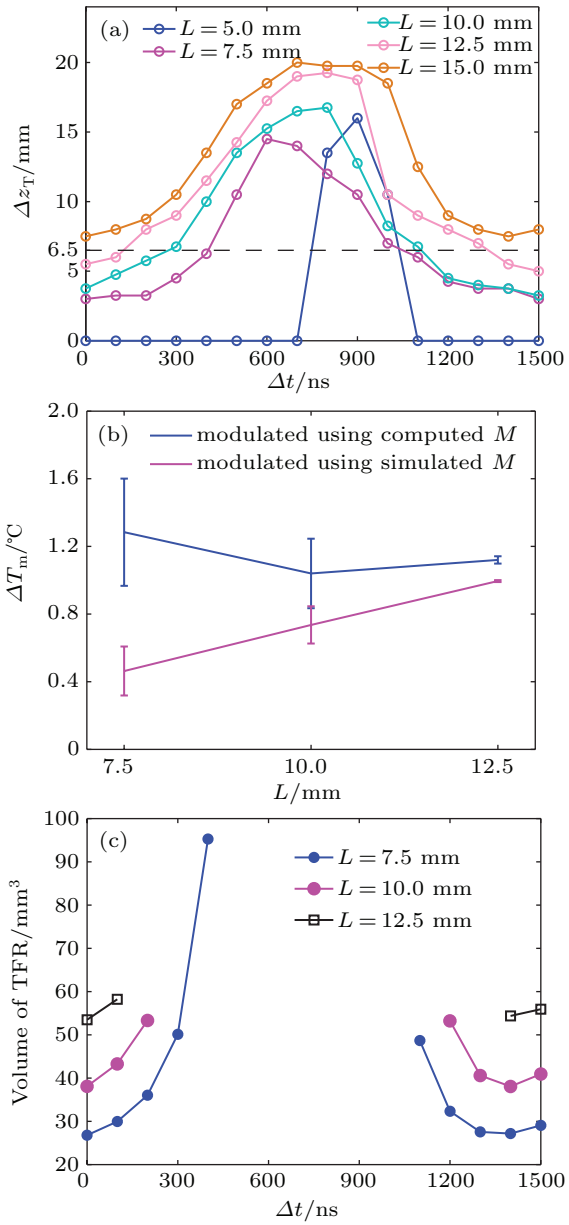


Fig. 8. (color online) (a) Variations of Δz_T with Δt under different L values ($P_w = 103.05$ W), (b) Variations of ΔT_m with L and (c) variation of TFR volume with Δt for different L values, with uniform temperature in the focal region, and maximum temperature of 65 °C.

3.2. Modulation with targets set to be at opposite side of acoustic axis

3.2.1. Modulation of thermal field by changing Δt

The modulation for generating a uniform temperature field in the direction perpendicular to the acoustic axis is implemented in this study. Take the case of F_1 located at (0, 1, 75), F_2 located at (0, −1, 75) and $L = 2.0$ mm (as shown in Fig. 2(b)) for example, figure 9 shows the temperature distributions with different Δt values when the maximum focal temperature reaches 65 °C ($P_w = 103.05$ W, $M = 0.50$). With Δt increasing from 0 to 1400 ns, the focal zone over 55 °C changes from one continuous area into two regions first, and then these two regions merge into one continuous area gradually.

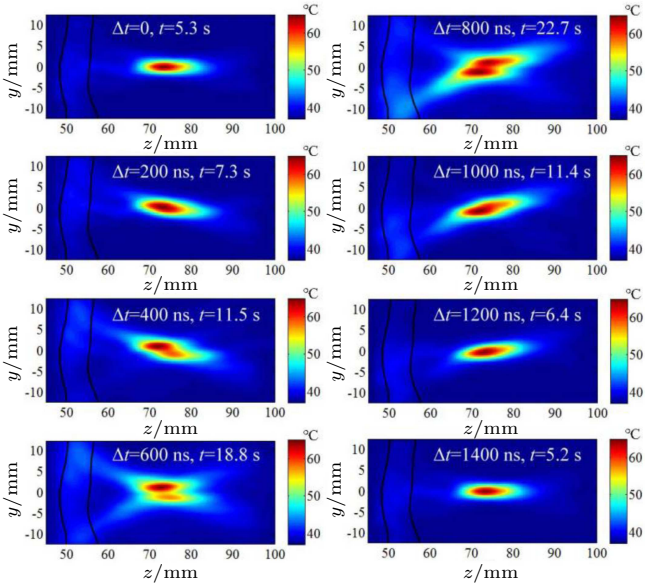


Fig. 9. (color online) Temperature distributions with different Δt values with targets set to be on opposite sides of the acoustic axis symmetrically and maximum focal temperature of 65 °C ($L = 2.0$ mm, $M = 0.50$, $P_w = 103.05$ W).

3.2.2. Modulation for generating uniform thermal field in direction perpendicular to acoustic axis

Figure 10 shows the temperature fields when F_1 is located at (0, 1, 75), F_2 is located at (0, −1, 75), $\Delta t = 400$ ns and the maximum focal temperature reaches 65 °C ($P_w = 103.05$ W) after amplitude modulation with $M = 0.45$. The temperature distribution on the y–z plane with $x = 0$ is shown in Fig. 10(a). The yellow areas in Figs. 10(b) and 10(c) show the cross sections of the focal region over 55 °C on the y–z plane and x–z plane. The temperature distribution in the y direction is nearly uniform with $\Delta T_m = 2.60$ °C. The shape of the focal region cross section on the y–z plane is a parallelogram with 9.00 × 4.00 mm (base × height) and it is an ellipse with 9.00 × 2.50 mm (major axis × minor axis) on the x–z plane.

The amplitude modulation is implemented based on the temperature distribution with $\Delta t = 1000$ ns as shown in Fig. 9, but no uniform temperature field is created. When the two targets are set to be F_1 (0, 1, 75), F_2 (0, −1, 77.5), and $M = 0.45$, the temperature field is shown in Fig. 11(a), where panel (a1) shows the temperature distribution on the y–z plane with $x = 0$ and panels (a2), (a3) show the cross sections of the focal region over 55 °C on the y–z plane and x–z plane, respectively. The temperature along the y direction is uniform with $\Delta T_m = 0.92$ °C and the shape of focal region cross section on the y–z plane is a parallelogram with 11.25 × 4.50 mm (base × height). Figure 11(b) shows the temperature field when F_2 moves to (0, −1, 80) and $M = 0.48$. The temperature along the y direction is uniform with $\Delta T_m = 0.13$ °C and the shape of focal region cross section on the y–z plane is a parallelogram with 13.25 × 5.00 mm (base × height).

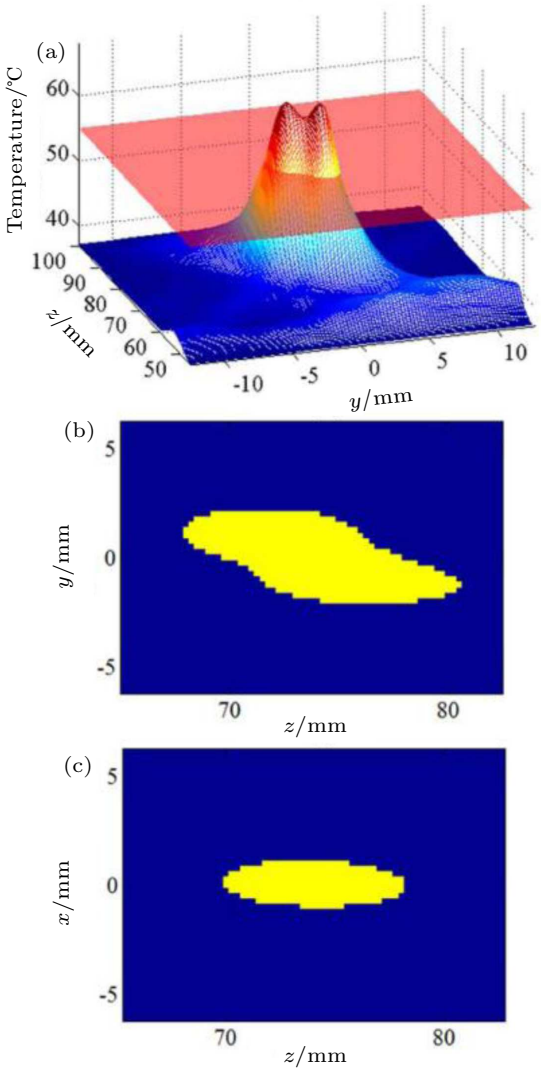


Fig. 10. (color online) Temperature fields with F_1 (0, 1, 75), F_2 (0, −1, 75), $\Delta t = 400$ ns, $M = 0.45$ and the maximum focal temperature of 65 °C ($P_w = 103.05$ W), showing (a) temperature distribution on the y–z plane of $x = 0$ and cross sections of the focal region (yellow area) over 55 °C on (b) y–z plane and (c) x–z plane respectively.

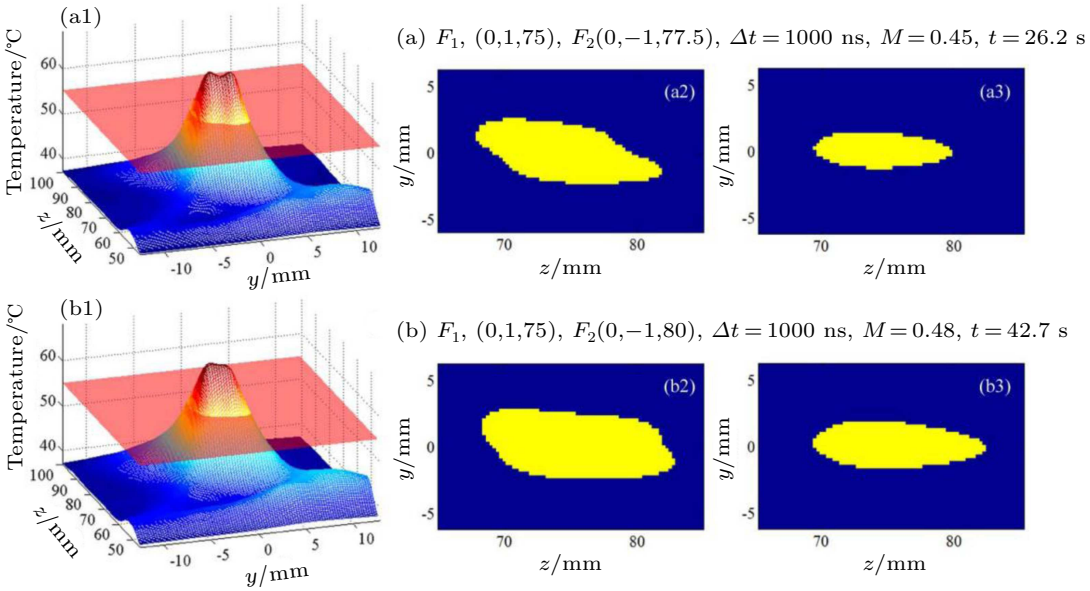


Fig. 11. (color online) Temperature field with F_1 set to be at (0, 1, 75) and F_2 set to be at different locations with uniform temperature distribution in the y direction and maximum focal temperature of 65 °C ($P_w = 103.05$ W). (a) F_2 (0, −1, 77.5), (b) F_2 (0, −1, 80).

3.2.3. Modulation for generating the uniform thermal field on *y* direction with different *L*

The targets are set as shown in Fig. 2(b) to modulate the temperature field in the focal region and the uniform temperature distribution in the y direction with $\Delta T_{\rm m} \leqslant 1$ °C is obtained when $L = 2.0$–3.0 mm. The parameters for generating the uniform temperature distribution are listed in Table 2. The short-axis of TFR in the y direction can be enlarged to more than 4.50 mm when the temperature distribution is uniform and the volume of TFR can be changed between 88.0 and 226.7 mm^3.

Table 2. Parameters for generating uniform temperature distribution along y direction and corresponding size of TFR ($P_{\rm w} = 103.05$ W).

L/mm	$^*L_z$/mm	Δt/ns	M	t/s	$\Delta T_{\rm m}$/°C	Size of TFR			
						x/mm	y/mm	z/mm	Volume/mm^3
2.00	2.50	1000	0.45	26.2	0.92	3.50	4.75	12.50	118.55
	5.00	1000	0.48	42.7	0.13	4.50	5.75	15.00	226.66
	−2.50	500	0.51	22.3	0.60	3.25	4.50	10.00	88.00
	−5.00	530	0.48	40.3	0.53	4.50	5.50	13.00	186.42
	2.50	150	0.47	23.0	0.64	3.25	5.00	13.75	119.89
3.00	5.00	200	0.49	33.5	0.69	4.25	5.75	15.50	198.06
	−2.50	1100	0.52	31.0	0.98	4.00	5.50	13.75	158.17

$^*L_z = Z_{F_2} - Z_{F_1}$, where Z_{F_1} and Z_{F_2} are the z coordinate values of F_1 and F_2, respectively.

4. Discussion

When the ultrasound wave propagates in skull, the mode conversion to shear waves is ignored in this study as most of the incident angles are less than 20° and the maximal incident angle is less than 25°.[10,43] The simulation model is established based on the CT data of a healthy volunteer's head, which is justified by the fact that there is no significant difference in acoustic parameter between tumor and brain tissue.[44]

In this study, a method to modulate the temperature distribution and generate a focal region with uniform temperature distribution is developed. Two drive signals that focus on two preset different targets are superimposed. The trigging time delay and amplitudes of the two signals are adjusted to achieve the focal region modulation. Using a single focus of HIFU, the temperature distribution and volume of the focal region are able to be adjusted by changing the acoustic power or irradiation time.[45,46] On the other hand, it carries a potential risk of damaging the normal tissue on the path of ultrasound beam.[47–49] The temperature distribution and volume of the focal region can be changed in soft tissue by electronic beam steering or multi-foci sonication[28,32,34,35] using a phased array transducer. In this study, transcranial HIFU focus modulation is accomplished. The temperature distribution, length of long axis, short axis as well as the volume of the focal region are able to be modulated by this method. The uniform temperature distribution along the acoustic axis is realized by setting the minimal distance between the superficial target and the inner surface of the skull to be 10 mm. Also, the uniform temperature distribution on the y axis is achieved by setting the minimal distance between the superficial target and the inner surface of the skull to be 12.5 mm (Fig. 12).

To improve the treatment efficacy of HIFU, Fan and Hynynen proposed that the temperature rise should be uniform in the focal region during the ultrasound irradiation.[50]

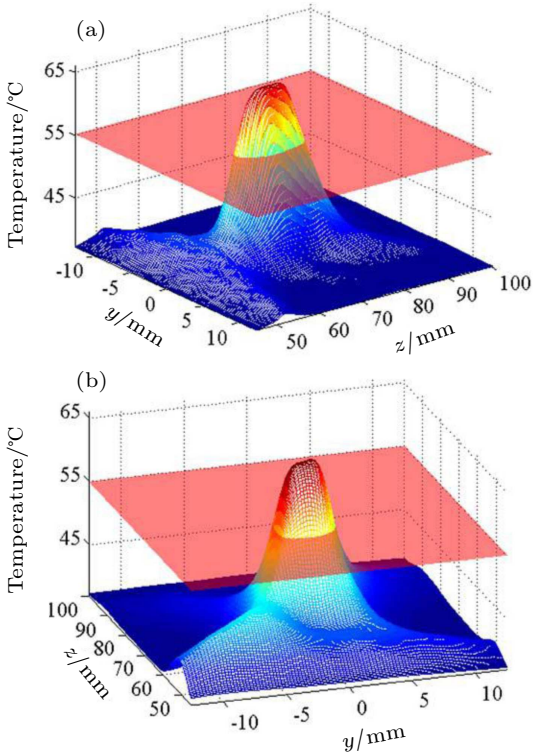


Fig. 12. (color online) Uniform temperature distributions in the direction of acoustic axis and y axis ($P_{\rm w} = 103.05$ W). (a) In the direction of acoustic axis with F_1 (0, 0, 65), F_2 (0, 0, 75) and (b) in y direction with F_1 (0, 1, 67.5), and F_2 (0, −1, 72.5).

Salomir *et al.* obtained a uniform temperature within a large target volume in the homogenous polyacrylamide gel and fresh meat samples using a double spiral trajectory of the transducer focal point.[29] Zhou attempted to obtain uniformly distributed ultrasound energy in the target area by optimizing the irradiation path and time interval between irradiations in his study using bovine liver.[33] However, the temperature modulation in transcranial HIFU has not been well studied. In this study, a uniform distributed temperature field was created in the brain by modulating delay time and amplitudes of two

acoustic excitation signals. The focal region volume formed by one irradiation can be modulated effectively while avoiding overheating injury. The volume and temperature distribution of the focal region can be adjusted to meet the requirement of clinical treatment. Stacking the different sized focal region to cover the whole tumor is required in the treatment of a large tumor. The uniform temperature distribution along the direction of the acoustic axis can also be created when the targets were set both on one side of the acoustic axis and parallel with the acoustic axis (Fig. 13).

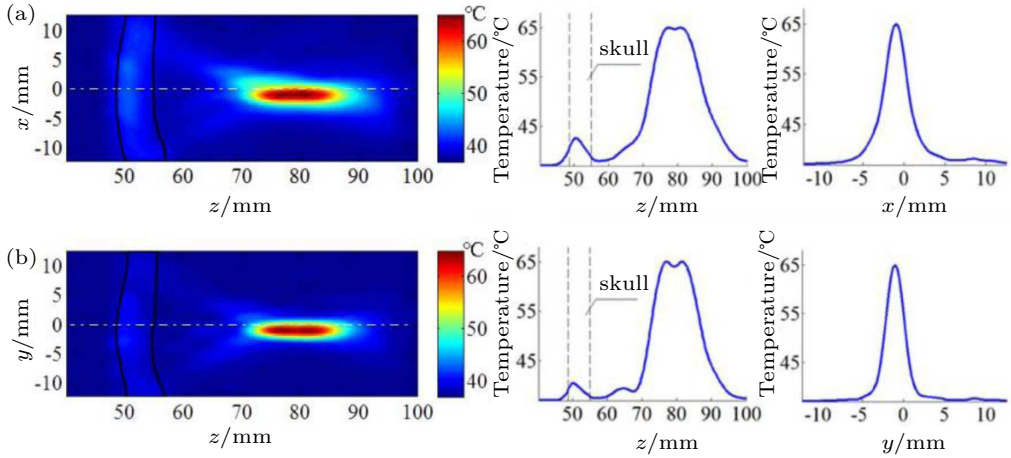


Fig. 13. (color online) Modulated results with the targets set to be off axis ($P_w = 103.05$ W), showing (a) temperature distribution on the x–z plane of $y = 0$, along the z direction and along the x direction across the position of maximum temperature for targets set to be at $(-1, 0, 75)$, $(-1, 0, 82.5)$, and (b) temperature distribution on the y–z plane of $x = 0$, along the z direction and along the y direction across position of maximum temperature with targets set to be $(0, -1, 75)$ and $(0, -1, 82.5)$.

The simulation results show that the range of L and $\triangle t$ for generating the uniform temperature distribution in the y direction are both narrow. The reason is that the length of the focal region in the vertical direction of the acoustic axis is short. The previous modulations of transcranial focusing were all completed based on the model as shown in Fig. 1. The distance between the inner surface of the skull and the transducer is 55 mm. In the case of setting both targets to be on the acoustic axis, the computed value of M based on Eq. (12) for $T_1 = T_2$ is consistent with the simulated value (Fig. 14) when the transducer moves toward the head and the distance between the inner surface of the skull and the transducer is 50 mm.

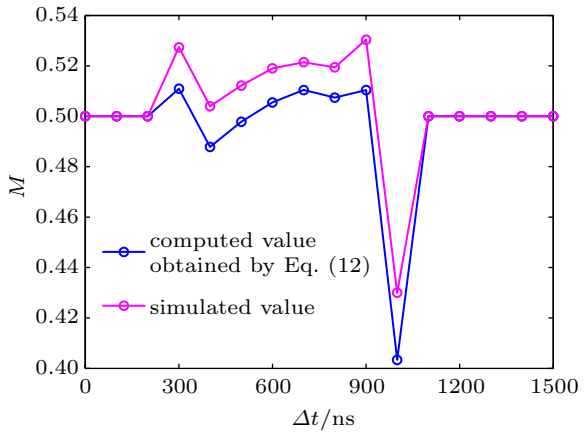


Fig. 14. (color online) Values of M for $T_1 = T_2$ with maximum temperature of 65 °C and 50-mm distance between the inner surface of the skull and the transducer ($L = 10.0$ mm, $P_w = 103.05$ W).

Connor and Hynynen indicated that no tissue exposed to less than an equivalent exposure of 30 min at 43 °C was damaged in the study on thermal deposition in the skull during transcranial HIFU treatment in 2004.[51] In Ding's work about the modulation of transcranial focusing thermal deposition in HIFU brain surgery, the temperature rise at the skull was controlled to be less than 10 °C.[10] In this study, the temperature of the skull is controlled to be below 47 °C when the modulation is carried out to generate a uniform temperature distribution in the focal region. Theoretically, it will not cause skull and surrounding tissues to be damaged. However, the cooling water circulation system is essential during the treatment. Using the double excitation signal superimposition technique, the location of the focus is mobile, however, a sidelobe is not observed when the modulation is implemented to generate the uniform temperature distribution in the focal region based on the simulation model used in this study. Further study in our laboratory will focus on the consistency of this method. Also the probability and potential solution of the sidelobe will be investigated.

5. Conclusions

The HIFU transcranial therapy research has shown that the best way to enhance the therapeutic efficacy is to control the shape and volume of the focal region and meanwhile to modulate the temperature distribution in the focal region to generate an ideal uniform temperature distribution. In this study a modulation method is proposed by superimposing double acoustic excitation signals. A series of numerical simulations is performed to calculate the thermal field which is formed by HIFU through superimposing a dual excitation signal.

The simulated results are as follows.

i) The uniform temperature distribution can be created in the direction along the acoustic axis and in the direction perpendicular to the acoustic axis as well (Figs. 7 and 11).

ii) The triggering delay time and the modulation coefficient of amplitude are two sensitive variables for modulating the thermal field (Figs. 3, 4, 9, and 10).

iii) The distance between the locations of the peak temperatures is an important parameter to determine whether a uniform temperature distribution can be generated.

iv) When the distance between the two preset targets is 7.5–12.5 mm with the targets both on the acoustic axis, the focal region with uniform temperature distribution (64–65 °C, $\Delta T_{\mathrm{m}} \leqslant 1$ °C) can be created by adjusting trigger time delay and the amplitudes of the two driving signals. The volume of treatable focal region formed by one single irradiation can be adjusted in a range of 26.8–95.3 mm^3. When the distance between the two preset targets is 2.0–3.0 mm with the two targets on the opposite side of the acoustic axis, a focal region with a uniform temperature distribution can be generated by the same technique, and the volume of treatable focal region formed by one irradiation can be adjusted in a range of 88.0–226.7 mm^3.

In summary, the numerical simulation results have verified that the new method proposed in this paper is capable of building a focal region with an effective treatable uniform temperature distribution. Also it can adjust the deposition volume of ultrasound energy during HIFU transcranial brain tumor treatment. We hope this method could improve the safety and efficacy of HIFU brain tumor therapy in the near future.

Acknowledgment

Numerical simulations were all performed on a Lenovo Think Station D30 workstation (Lenovo Group Ltd, Beijing, China) with an Nvidia TitanX GPU (NVIDIA Corporation, Santa Clara, California, US).

References

[1] Wang H L, Fan P F, Guo X S, Tu J, Ma Y and Zhang D 2016 *Chin. Phys. B* **25** 124314
[2] Yuan Y, Chen Y D and Li X L 2016 *Chin. Phys. B* **25** 084301
[3] Wang X D, Lin W J, Su C and Wang X M 2018 *Chin. Phys. B* **27** 024302
[4] Su H D, Guo G P, Ma Q Y, Tu J and Zhang D 2017 *Chin. Phys. B* **26** 054302
[5] Hsiao Y H, Kuo S J, Tsai H D, Chou M C and Yeh G P 2016 *J. Cancer* **7** 225
[6] Kennedy J E 2005 *Nat. Rev. Cancer* **5** 321
[7] ter Haar G 2007 *Prog. Biophys. Mol. Biol.* **93** 111
[8] Fry F J 1958 *Am. J. Phys. Med. Rehabil.* **37** 152
[9] Fry F J, Kossoff G, Eggleton R C and Dunn F 1970 *J. Acoust. Soc. Am.* **48** 1413
[10] Ding X, Wang Y Z, Zhang Q, Zhou W Z, Wang P G, Luo M Y and Jian X Q 2015 *Phys. Med. Biol.* **60** 3975
[11] Hynynen K and Jolesz F A 1998 *Ultrasound Med. Biol.* **24** 275
[12] Marquet F, Pernot M, Aubry J F, Montaldo G, Marsac L, Tanter M and Fink M 2009 *Phys. Med. Biol.* **54** 2597
[13] Narumi R, Matsuki K, Mitarai S, Azuma T, Okita K, Sasaki A, Yoshinaka K, Takagi S and Matsumoto Y 2013 *Jpn. J. Appl. Phys.* **52** 07HF01-1
[14] Thomas J L and Fink M A 1996 *IEEE Trans. Ultrason. Ferroelectr. Freq. Control* **43** 1122
[15] Tanter M, Thomas J L and Fink M 1998 *J. Acoust. Soc. Am.* **103** 2403
[16] Aubry J F, Tanter M, Pernot M, Thomas J L and Fink M 2003 *J. Acoust. Soc. Am.* **113** 84
[17] Pernot M, Aubry J F, Tanter M, Andre F and Fink M 2004 *IEEE Ultrason. Symp.*, 23–27 Aug, Montreal, Canada, p. 1005
[18] Sun J and Hynynen K 1998 *J. Acoust. Soc. Am.* **104** 1705
[19] Clement G T, Sun J, Giesecke T and Hynynen K 2000 *Phys. Med. Biol.* **45** 3707
[20] Leduc N, Okita K, Sugiyama K, Takagi S and Matsumoto Y 2012 *J. Biomech. Sci. Eng.* **7** 43
[21] Coluccia D, Fandino J, Schwyzer L, O'Gorman R, Remonda L, Anon J, Martin E and Werner B 2014 *J. Ther. Ultrasound* **2** 17
[22] Jeanmonod D, Werner B, Morel A, Michels L, Zadicario E, Schiff G and Martin E 2012 *Neurosurg. Focus.* **32** E1
[23] Chang W S, Jung H H, Kweon E J, Zadicario E, Rachmilevitch I and Chang J W 2015 *J. Neurol. Neurosurg. Psychiatr* **86** 257
[24] Elias W J, Huss D, Voss T, Loomba J, Khaled M, Zadicario E, Frysinger R C, Sperling S A, Wylie S, Monteith S J, Druzgal J, Shah B B, Harrison M and Wintermark M 2013 *N. Engl. J. Med.* **369** 640
[25] McDannold N, Clement G T, Black P, Jolesz F and Hynynen K 2010 *Neurosurgery* **66** 323
[26] Martin E and Jolesz F A 2011 *Tumors of the Central Nervous System* (Dordrecht: Springer Netherlands) pp. 227–236
[27] Magara A, Buhler R, Moser D, Kowalski M, Pourtehrani P and Jeanmonod D 2014 *J. Ther. Ultrasound* **2** 11
[28] Ebbini E S and Cain C A 1989 *IEEE Trans. Ultrason. Ferroelectr. Freq. Control* **36** 540
[29] Salomir R, Palussiere J, Vimeux F C, de Zwart J A, Quesson B, Gauchet M, Lelong P, Pergrale J, Grenier N and Moonen C T 2000 *J. Magn. Reson. Imaging* **12** 571
[30] Lu M Z, Wan M X, Shi Y and Song Y C 2002 *Acta Phys. Sin.* **51** 928 (in Chinese)
[31] Xu F, Lu M Z, Wan M X and Fang F 2010 *Acta Phys. Sin.* **59** 1349 (in Chinese)
[32] Partanen A, Tillander M, Yarmolenko P S, Wood B J, Dreher M R and Kohler M O 2013 *Med. Phys.* **40** 013301-1
[33] Zhou Y F 2013 *Ultrasonics* **53** 495
[34] Kohler M O, Mougenot C, Quesson B, Enholm J, Le Bail B, Laurent C, Moonen C T and Ehnholm G J 2009 *Med. Phys.* **36** 3521
[35] Vincenot J, Melodelima D, Chavrier F, Vignot A, Kocot A and Chapelon J Y 2013 *Ultrasound Med. Biol.* **39** 1241
[36] Lee K I, Sim I, Kang G S and Choi M J 2008 *Mod. Phys. Lett. B* **22** 803
[37] Westervelt P J 1963 *J. Acoust. Soc. Am.* **35** 535
[38] Hallaj I M, Clevel and R O 1999 *J. Acoust. Soc. Am.* **105** L7
[39] Pennes H H 1948 *J. Appl. Physiol.* **1** 93
[40] Sapareto S A and Dewey W C 1984 *Int. J. Radiat. Oncol. Biol. Phys.* **10** 787
[41] Vykhodtseva N, Sorrentino V, Jolesz F A, Bronson R T and Hynynen K 2000 *Ultrasound Med. Biol.* **26** 871
[42] Pinton G, Aubry J F, Fink M and Tanter M 2011 *Med. Phys.* **38** 1207
[43] Clement G T, White P J and Hynynen K 2004 *J. Acoust. Soc. Am.* **115** 1356
[44] Tao M H 2016 *The Numerical Simulation Study on Treatable Focal Region of Transcranial Brain Tumor with High-intensity Focused Ultrasound* (MS Thesis) (Tianjin: Tianjin Medical University) (in Chinese)
[45] Chauvet D, Marsac L, Pernot M, Boch A L, Guillevin R, Salameh N, Souris L, Darrasse L, Fink M, Tanter M and Aubry J F 2013 *J. Neurosurg.* **118** 1046
[46] Eames M D, Hananel A, Snell J W, Kassell N F and Aubry J F 2014 *J. Ther. Ultrasound* **1** 24
[47] Ghanouni P, Dobrotwir A, Bazzocchi A, Bucknor M, Bitton R, Rosenberg J, Telischak K, Busacca M, Ferrari S, Albisinni U, Walters S, Gold G, Ganjoo K, Napoli A, Pauly K B and Avedian R 2017 *Eur. Radiol.* **27** 732
[48] Li J J, Gu M F, Luo G Y, Liu L Z, Zhang R and Xu G L 2009 *Technol. Cancer Res. Treat* **8** 217
[49] Zhang Y, Aubry J F, Zhang J, Wang Y, Roy J, Mata J F, Miller W, Dumont E, Xie M, Lee K, Zuo Z and Wintermark M 2015 *Ultrasound Med. Biol.* **41** 449
[50] Fan X and Hynynen K 1996 *Ultrasound Med. Biol.* **22** 471
[51] Connor C W and Hynynen K 2004 *IEEE Trans. Biomed. Eng.* **51** 1693